Optical scintillation observed from a “redback” millisecond pulsar

André van Staden
Observatory code 641
Overberg, South Africa
andre@etiming.co.za

Abstract: PSR J1723-2837, is a “redback” millisecond pulsar (MSP) with a non-degenerative low mass companion in a 14.8 hr orbit. The presented paper is a followed-up report on a long-term, time-series photometry campaign of the 15.5 magnitude companion to the pulsar. In a previous paper we showed that the star experiences episodes of sporadic stellar activity and is not tidally locked. In this paper the author reports on small (σ ≈ 5.8 mmag) scattered noise, superimposed on the companion’s light curve. These rapid fluctuations were observed during 2018 and predominantly coincided at superior conjunction when the pulsar was behind the companion. To the author’s knowledge, similar phenomena in optical have not been observed to date in other MSP systems.

"In science, one man's noise is another man's signal."
Edward Ng

1. Introduction

Since the discovery of the first pulsar in 1967 by Jocelyn Bell Burnell and Antony Hewish, pulsars have captivated our imagination and have many unique applications for example in testing theories such as general relativity. The first millisecond pulsar (MSP), PSR B1937+21, was discovered in 1982 by D.C. Backer et al, spinning roughly 641 times a second (Backer et al. 1982). Common properties of MSPs with a binary companion are radio eclipses around superior conjunction (i.e., when the pulsar is behind the companion), γ-and X-ray emission, rapid orbital-period modulations, and strong optical variability (Archibald et al. 2013). Eclipsing MSPs are commonly classified as either "black widows" or "redbacks," depending on the mass of the companion (m_c of up to few $10^{-2}M_\odot$ and $m_c \simeq 0.2\text{-}0.7M_\odot$, respectively).

PSR J1723-2837 is a redback, 1.86 MSP in an almost circular ≈14.8 hour orbit, about a main-sequence-like companion star discovered by Faulkner et al. (2004) in the Parkes Multibeam survey. The Companion star (J17232318-2837571) was first identified using Infrared, optical, ultraviolet and spectrophotometry (Crawford, 2013). X-Ray emissions were also detected from PSR J1723–2837 and are presumably a candidate for a radio pulsar/X-ray binary transition object (Bogdanov, 2014), (Hui et al, 2015).

Secular changes in average photometric flux of the companion stars to redbacks and BW pulsars are quite common but proved to be challenging to explain with limited observation times granted to Astronomers. PSR J1723–2837 has a bright (V 15.5 mean magnitude) optical counterpart, making it an ideal case-study for redback MSPs. In this context, the author initialized a long-term intensive photometry campaign (starting in 2014) with the objective to obtain a consistent light curve in support of MSP studies.

In order to achieve a logical order regarding the reporting of observations and data in this paper, the results will be presented in the following manner. Firstly, as reports on observations obtained during 2018 containing scattered "noise" besides the normal photometry variations. Then it will be shown that the scattering power was more intense during phases of superior conjunction when the pulsar was behind the companion. Finally it will be shown that the scattered power also responded to frequency bandwidths, manifesting at both superior and inferior conjunctions.

2 Observations and Photometric Reduction

The companion to PSR J1723−2837 was observed between 3 August 2014 and 8 June 2019 from Overberg, South Africa. The location of the observatory allows for continuous monitoring of the target for up to 9 hrs per night, or 60% of the orbital

period. The site suffers from minimal light pollution and the seeing typically ranges from 2 to 3 arcsec.

All observations were conducted with a 30 cm Cassegrain telescope and a commercial SBIG ST9e CCD camera cooled to -15°C, with 20μm^2 pixels arranged in a 512 × 512 grid. Guiding corrections were performed with the integrated tracking CCD at 1 sec intervals, always using the same star. The images were calibrated using standard dark and sky-flat frames acquired sporadically throughout the campaign.

More than 8000 images were collected over 175 nights (hereafter referred to as datasets), with exposure times of 300 seconds, except for 2015 when exposure times were 600 seconds. The images were reduced, based on visual inspection followed by a software routine that rejects images with large FWHM mainly caused by defocusing as a result of temperature fluctuations during the night, rapid sky background changes caused by high clouds and standard error estimates by C-Munnipack, bringing the final images used in this report to ≈6000.

The magnitudes reported are based on differential ensemble type aperture photometry, computed with C-Munipack/Muniwin v. 2.0.17 (http://c-munipack.sourceforge.net/), a public photometry program. Fluxes were measured inside an aperture enclosing twice the FWHM of the local PSF, and the sky was extracted from a surrounding region up to five times the FWHM, but excluding the area close to the source, which contains a faint star. The author experimented with different settings, each time extracting consistent results. A set of twenty bright objects were selected to derive a virtual comparison star. The target object was only ≈4.3° from the Galactic plane, therefore resulting in over 2000 stars in the 18x18 arcminute images, making it impossible to obtain clear sky annulus for all the selected stars. An algorithm was developed for superimposing uniform sky annulus onto the CCD images, surrounding the “comparison stars” based on statistical information of the sky background. Additionally, the virtual comparison star was calculated, based on a weighted arithmetic mean within an iterative loop, rejecting the comparison stars with the largest noise components. This additional process delivered consistent results compared to the standard reduction provided by C-Munipack with marginal improvements at times. However the results reported in this paper were produced by the standard C-Munipack package that uses the Robust Mean Algorithm based on a re-descending Ψ type M-estimator for calculating the sky background.

To be on the conservative side and further improve the photometric S/N ratio, neighboring measurements (in time) were averaged. Therefore each combined measurement resembles an approximately integration time of 600 seconds. This technique was found to produce slightly lower rms noise values compared to single

600 second exposures. RMS values for a close by star were computed for each dataset producing a mean RMS for all sets of ≈2.7 mmag as shown in figure 1.

Time stamps were derived from PC time, which was synchronized to an international time server and checked regularly against a GPS master clock. All measurements were referred to Heliocentric times derived from the center of exposures. Binary phases were calculated using the pulsar timing ephemeris of Crawford et al. (2013), adopting Tasc=MJD 55425.320466(2) for the time of ascending node and Pb= 0.615436473(8) days for the orbital period. The author also accounts for the small secular change in the orbital period, $\dot{P}b \simeq -3.50(12)\times10^{-9}$, which could result in a delay of up to $\Delta Pb > -0.5$ sec over the span of the observations. Higher-order variations in Pb were omitted, as their effect are too small to influence the results (Crawford et al. 2013). Under the adopted convention, $\phi=0.25$ coincides with the superior conjunction, when the pulsar is eclipsed by its companion in radio frequencies.

3 Data Analysis And Results

3.1 Optical variability of the companion to PSR J1723-2837

The optical light curve of the companion to PSR J1723-2837 is similar to a number of binary MSPs that show double peaked ellipsoidal variation as a result of the tidal distorted geometry caused by the gravitational pull of the MSP. No significant traces of irradiation were observed during the campaign. The ellipsoidal signal, modulated at the first orbital harmonic has an average amplitude of ≈0.0512 magnitudes. However, it was found that there were periods (>10 months) with alternating dimming at $\phi \approx 0.25$ and $\phi \approx 0.75$ which will be addressed in a future paper. Dips drifting across the light curve up to ≈0.1 magnitudes were observed during 2015 and early 2016 which were attributed to starspots (van Staden & Antoniadis, 2016). This caused fluctuations on timescales of weeks to months. Random fluctuations on time scales of weeks to days were occasionally seen throughout the campaign. Interestingly, these fluctuation were more frequently observed between $\phi=0$ and $\phi=0.25$, especially during 2018. Roughly speaking, the quietest periods up to date were 2014 and 2017.

3.2 RMS of scattered noise

The remainder of this paper focused on scintillation discovered in optical observations during 2018. The scintillation was mostly composed of sporadic outliers and rapid fluctuations (generally referred to as scattered noise in this paper) with periods P_n <2hr, superimposed on the light curve. In section 3.4 it was shown that the scintillation also contains periodicities at times. It should be noted that the magnitude of these signals were only a fraction of the ellipsoidal variations.

The first step was to separate and quantify the amount of scattering (P_n<2hr) from other variations in the light curve. The scatter was defined by the difference between the measured light curve (LC_{meas}) and the estimated ellipsoidal signal plus secular variations (>12 Cycles/d (P≃2h) which might have been caused by star spots and/or other unknown effects. These fluctuations were approximated by best fitted polynomials where the order was adapted to the duration of the datasets. As a mathematical equation, the scattered noise or residue, Y_{res} was expressed as:

$$Y_{res} = LC_{meas} - (A \cdot \cos(4\pi \cdot f \cdot t) + p(x))$$

Where:
A = 0.0590 mag, Ellipsoidal magnitude estimated by a least square fit and Fourier Analyses (see also van Staden & Antoniadis, 2016)
f = 1.6248630, Orbital frequency from published radio ephemeris (see Crawford et al. 2013)
t = time, CCD heliocentric timestamps
$p(x) = p_1 x^n + p_2 x^{n-1} +...+ p_n x + p_{n+1}$, where p(x) is a polynomial of degree n that is a best fit (in a least-squares sense) for the data, and $2 \leq n \leq 6$. (The roll-off filtering-effect was verified with Fourier Analyses to be consistently at P_n≃2hrs)

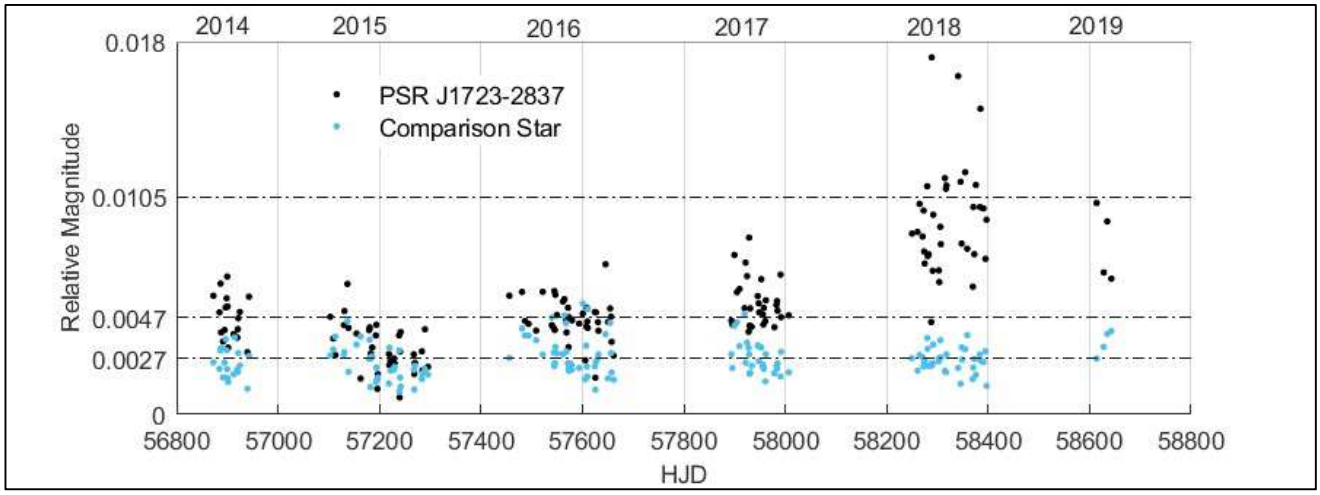

Fig 1. Each dot in the graph represents an rms scatter value for nightly observations. The Comparison star's (blue dots) had a mean rms of 0.0027 magnitudes while PSR J1723-2837 (black dots) was estimated at 0.0047 and 0.0105 magnitudes for 2014-2017 and 2018, respectively.

For each dataset from 2014 to 2019, rms values were computed from the residues (Y_{res}) and plotted in figure 1 as black dots. Rms values were also determined for a comparison star (≈1 magnitude brighter) close to PSR J1723-2837 and were plotted with blue dots in figure1. The average (Y_{res}) rms for PSR J1723-2837 from 2014 to 2017 was 0.0047 magnitudes and 0.0105 magnitudes during 2018. In contrast, the

comparison star remained constant during the campaign with an average rms value of 0.0027 magnitudes.

3.3 The spectrum of the scattered signal

The power spectrum densities (PSD) determined from residues (Y_{res}), before and during 2018 were computed by means of a Lomb–Scargle periodogram (Lomb 1976; Scargle 1982). Firstly, the Y_{res} spectra for all 136 datasets before 2018 were computed and average combined. The result was plotted as a red curve in figure 2 which shown a reasonable flat spectrum with a roll-off at ≈12 Cycles/d (P≃2h) as a result of the polynomial filtering effect.

The process was repeated for datasets obtain only during 2018 with result shown in Fig. 2 (black curve). The much higher power in the spectrum was consistent with the rms scatter increase during 2018 (see section 3.2). Also notable were two (marginal) peaks at ≈27 cycles□d^{-1} (P≃53 minutes) and ≈40 cycles□d^{-1} (P≃36 minutes). The power associated with the peaks was covered in section 3.4. For comparison, the average combined spectrum of the comparison star from 2014 to 2018 was computed and also plotted in Fig 2 (blue) which showed reasonable consistency (from ≈10-70 cycles□d^{-1}) with white noise.

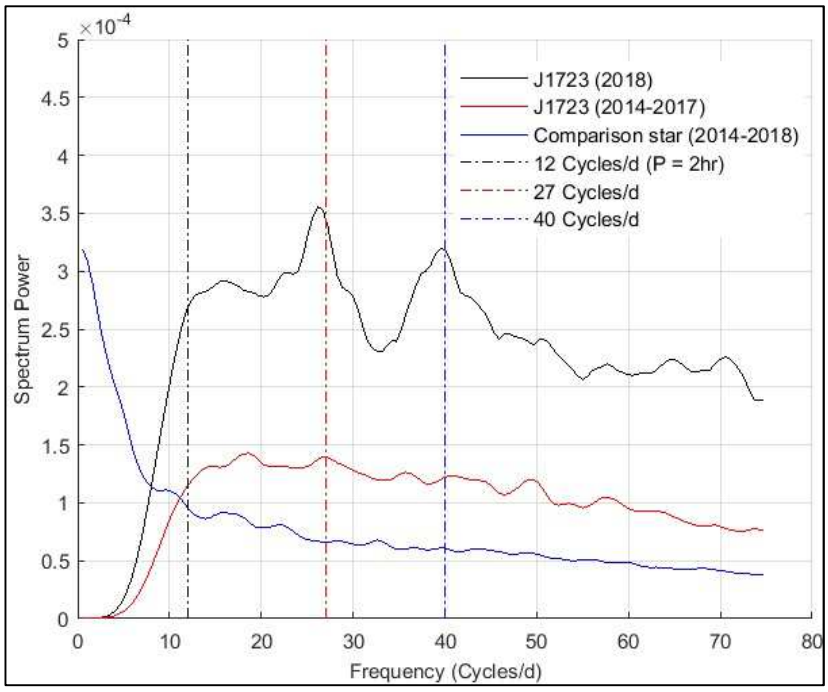

Fig 2. Average combined power spectrum density (PSD) for three instances. The black and red curve represented the scatter observed from PSR J1723-2837 during 2018 and 2014-2017 respectively. The blue curve represented the PSD for a comparison star (2014-2018). The two peaks shown up in the black curve at ≈27 cycles□d^{-1} and ≈40 cycles□d^{-1} were marked with vertical dashed lines. The "roll-off" as discussed was at ≈12 cycles□d^{-1}.

3.4 Scattered power in relation to orbital phase

Various methods were examined to see if the scatterings were evenly distributed throughout orbital rotation.

The best results were obtained by looking for the scattered power contents in narrow frequency bands, thus improving the Signal-to-Noise ratio. Special preference was given to the power peaks mentioned at ≈27 cycles□d^{-1} and ≈40 cycles□d^{-1} and were incorporated into a band-pass filtering scheme as follows:

Y_{res} data (2014-2018) were loaded consecutively into bins followed by a PSD's calculation per bin. The total power was determined by combining the average of all the PSD-magnitudes within a selectable bandwidth. The total power was then normalized by scaling to the size of the bandwidth used. The relevant orbital phases were calculated from the Y_{res} timing information that coincided with the centre of each bin. The product of this algorithm was consequently an array of power values with related phase values.

Three computations were performed in this manner with bandwidths set consecutively to 24-31, 35-45 and 50-80 cycles.d^{-1} and were presented in figure 3 (black circles) as power vs orbital phase plots.

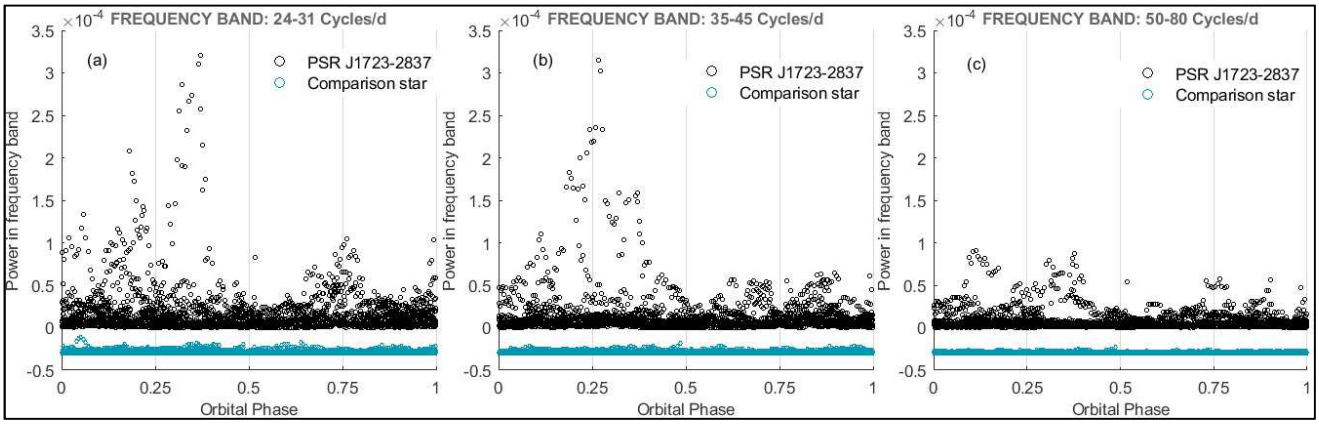

Fig 3. Bandwidth limited Spectral Power in relation to Orbital phase (2014 – 2018). (a) PSD for bandwidths set to 24-31 cycles.d^{-1}, (b) 35-45 cycles.d^{-1} and (c) 50-80 cycles.d^{-1}. PSR J1723-2837 and a comparison star were presented as black and blue circles, respectively.

Evident from Figs 3(a) and 3(b) were the power peaks at $\phi \simeq 0.25$ *and* much smaller peak at $\phi \simeq 0.75$ when pulsar was in front of the companion (figure 3a). With the bandwidth set to 50-80 cycles.d^{-1}, shown in figure 3(c), the power peaks became relatively insignificant. This is a clear indication that a) maximum scattering coincided at $\phi \simeq 0.25$ (and possibly $\phi \simeq 0.75$) and b) the scattering probably contained periodicities that also coincided with the mentioned orbital phases.

As a controlled check, the process was repeated for the same period on the comparison star and was plotted with blue circles (with an intentionally set offset). In

all instances, the comparison star showed reduced and evenly distributed power as expected.

4 Conclusion

The companion to PSR J1723-2837 has an optical light curve dominated by tidal distortion (ellipsoidal modulation) over possible heating from the pulsar. During a long-term intensive monitoring campaign by the author, it became apparent that the companion star is probably magnetic active, producing complex light curves at times during episodes of star spots.

A scintillating effect was discovered in photometric observations made during 2018 that resulted in an increase in rms scatter from 4.7 mmag (2014-2017) to 10.5 mmag (2018) obtained from more than 6000 images in total. These scattered photometric noises were mostly composed of sporadic outliers and fluctuations with short periods (on time scales of minutes) superimposed on the ellipsoidal and other variations.

From the data it was discovered that the power in the scattered signal was significantly more prominent during phases of superior conjunction when the pulsar was behind the companion star. This suggests an interesting scenario in support of emission probably not originating from the companion star but probably an interaction between the two objects e.g. accretion flow, accretion disk or jets. Considering the inferred orbital inclination angle of 41° by Crawford (2013), it may further suggest emissions close to the MSP for producing the concentrated scattering power observed at $\phi \simeq 0.25$. Taking into account the marginal increase in scattering at $\phi \simeq 0.75$ (Figure 3a) when the pulsar was in front of the companion, is even more intriguing.

Finally it was shown that the increase in scattered power coincided with specific frequency bands, roughly in the order of $\approx$27 cycles.d^{-1} and $\approx$40 cycles.d^{-1}. Taking these frequencies at face value, is an interesting question why periodicities were associated with the emission in the first place.

Related optical variability was looked for in literature but without much success. However, the author would like to point out the work done by [Gandhi 2009] who investigated and confirmed the relationship of optical variability vs flux in X-ray of X-ray binaries. Although this seems promising, it should be noted that previous X-ray observations for PSR J1723-2837 showed a minimum X-Ray flux during $\phi \simeq 0.25$ (Bogdanov, 2014; Hui, 2015), making it less favorable to explain.

The emitting source and reason(s) for fluctuations observed are unclear at this point in time. Filtered observations will be helpful but will require a larger telescope.

Simultaneous observations in other frequencies will be very interesting and the author hopes that this work will encourage more research and future observations.

References

Archibald, A. M., Kaspi, V. M., Hessels, J. W. T., et al. 2013, ArXiv e-prints, arXiv:1311.5161
Backer, D. C., et al., 1982, *Nature*, **300**, 615
Bogdanov S., et al., 2014, *ApJ*, **781**, 6
Crawford F., et al., 2013, *ApJ*, **776**, 20
Faulkner, A. J., Stairs, I. H., Kramer, M., et al. 2004, *MNRAS*, **355**, 147
Gandhi P., 2009, *ApJ*, **697**, L167
Gandhi P. et al., 2010, *MNRAS*, **407**, 2166
Hui, C. Y., Hu, C. P., Park, S. M., et al., 2015, *ApJL*, **801**, 27
Lomb, N. R. 1976, *Ap&SS*, **39**, 447
van Staden, A. D., & Antoniadis, J. 2016, *ApJL*, **833**, L12